



surface predicted the presence of several surface-state bands with primarily  $d$  character localized on the Ni atoms. The investigation of these surface states, both experimentally and theoretically, could lead to an understanding of the chemical and physical properties of this alloy surface and help to elucidate the general questions pertaining to multicomponent surfaces. This system is of particular interest because a change in the electronic configuration of the surface Ni atoms could produce a magnetic surface layer (bulk NiAl is nonmagnetic<sup>12</sup>). In this paper, we address these questions by comparing measured surface bands with calculated surface states. Bulk and surface features are measured by angle-resolved photoemission both at the surface zone center and along the high symmetry lines in the surface zone. The calculation of surface states is carried out using the experimental relaxed geometry.<sup>1,2</sup>

As an introduction to the properties of bulk NiAl, Fig. 2(a) shows the bulk total density of states (DOS). The dominant peak in Fig. 2(a), the Ni  $d$  states, centers at  $-2.0$  eV while its tail extends slightly above the Fermi energy with a depletion of state density at  $-1$  eV. The second largest contribution to the total DOS is the  $p$ -like states on the Al site centered around  $-3$  to  $-4$  eV. The  $p$ -like states also dominate the portion of DOS at and near the Fermi level. The Al  $s$ -like states are confined almost exclusively to low energies. We note that the shape and the peak position of the completely filled  $d$  bands in the DOS of NiAl resembles that of elemental copper much more than that of pure Ni.<sup>13</sup> The calculated bulk band structure can be used to obtain a projection of the bulk states onto the surface Brillouin zone (SBZ). Figure 2(b) shows the projection of the even electronic states along the  $\bar{X}-\bar{\Gamma}-\bar{Y}$  direction. In this projection, most of the band gaps present are in the energy region of the  $d$  band, i.e., between  $-1.0$  and  $-3.0$  eV as well as in the

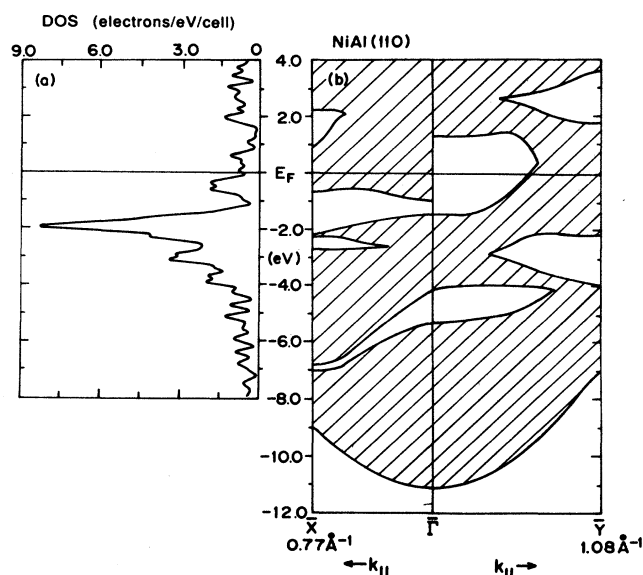


FIG. 2. (a) Total density of states of bulk NiAl. (b) Bulk projections of even electronic states along  $\bar{X}-\bar{\Gamma}-\bar{Y}$ .

region of the  $s$  band. The calculations predict that surface and resonance states with  $d$  character exist in the energy range of the  $d$  band. Their energy and wavefunction symmetry will be discussed and compared to the measured surface states.

The bulk band structure of NiAl(110) has been measured using angle-resolved photoemission with synchrotron radiation.<sup>6</sup> The high symmetry points of the bulk bands are obtained from such measurements and have been compared with the present theory. This comparison between theory and experiment shows a measured bulk  $d$ -band narrowing of 16% and this difference is consistent with other local-density-approximation (LDA) calculations for NiAl.<sup>14</sup> For normal emission the measurement probes bulk states along the  $\Sigma$  symmetry line, and the allowed dipole transitions are from initial states with  $\Sigma_1$ ,  $\Sigma_3$ , and  $\Sigma_4$  symmetry. Figure 3 displays the normal emission  $s$ -polarized photoemission spectra from the  $\Sigma_3$  and  $\Sigma_4$  initial states and the  $p$ -polarized  $\Sigma_1$  initial states. Transitions from the  $\Sigma_2$  initial band are forbidden by symmetry in normal emission. In Fig. 3 bulk bands are indicated by arrows and surface-state peaks are shaded and labeled according to their symmetry. A bulk band is

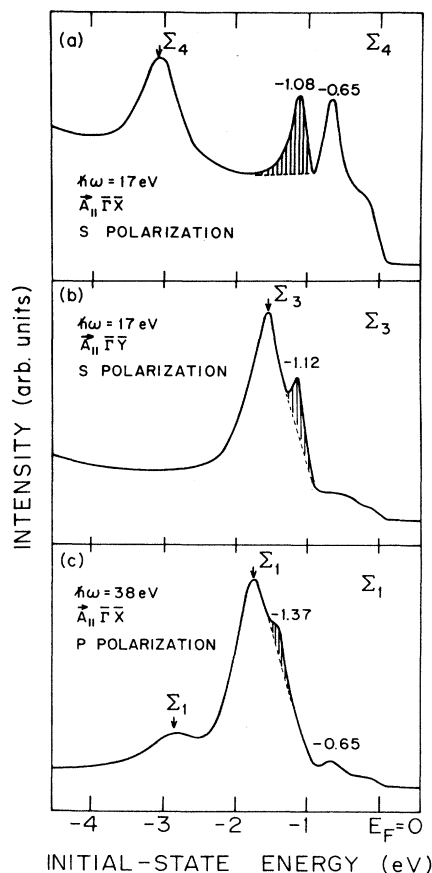


FIG. 3. Normal emission EDC's showing initial-state bands with (a)  $\Sigma_4$ , (b)  $\Sigma_3$ , and (c)  $\Sigma_1$  symmetries. Surface states are shaded peaks and bulk transitions are indicated by arrows.

identified by its motion in initial state energy as the photon energy is changed.<sup>14</sup>

There are two remarks about the photoemission spectrum for the  $\Sigma_4$  initial state shown in Fig. 3(a). First, the peak at  $-0.65$  eV which is as intense as the  $-1.08$  eV surface state is not assigned to be a surface state, its character will be discussed in Sec. III C. Second, since the transition of the bulk  $\Sigma_1$  band is very strong, it also appears in the  $s$ -polarized spectrum taken with  $10^\circ$  incident angle. At this angle, the component of the vector potential ( $\mathbf{A}$ ) of the light along the surface normal is nonzero. To show initial states with only  $\Sigma_4$  symmetry as the one displaced in Fig. 3(a), the  $\Sigma_1$  peak is subtracted from the  $s$ -polarized spectrum. The shaded peaks in Figs. 3(a)–3(c) are nondispersive with changing photon energy, but show well-defined symmetry. They are indicated in Fig. 3 as surface states with binding energies as follows:  $\Sigma_1$  at  $-1.37$  eV,  $\Sigma_3$  at  $-1.12$  eV, and  $\Sigma_4$  at  $-1.08$  eV. Their character, dispersion, symmetry, and cross sections will be discussed in Sec. III.

## II. EXPERIMENTAL AND THEORETICAL PROCEDURES

The angle-resolved photoemission experiment on NiAl(110) was carried out at the National Synchrotron Light Source (NSLS) at Brookhaven National Laboratory (Upton, NY). Radiation from the 750-MeV VUV storage ring was dispersed by a dual toroidal grating monochromator yielding photons in the  $10 < \hbar\omega < 120$  eV range.<sup>15</sup> Photoelectrons were energy analyzed with a hemispherical electrostatic analyzer with an acceptance angle of  $\pm 2^\circ$ . The combined instrumental resolution (photon and electron) is  $\sim 0.13$  eV for  $\hbar\omega < 35$  eV and increases linearly with photon energy to  $\sim 0.30$  eV at  $\hbar\omega = 60$  eV. The details of the angle-resolved analyzer and the experimental chamber were described elsewhere.<sup>16</sup> The crystal was cleaned by cycles of neon ion bombardment followed by annealing to  $850^\circ\text{C}$  to restore a well-ordered  $(1 \times 1)$  surface as indicated by LEED. The average surface composition of the sample<sup>9</sup> is known to be similar to the bulk composition which is near stoichiometry ( $50.6 \pm 2.0$  at. % Al). This composition was determined by Paschen optical emission spectroscopy and the use of standard solutions. In addition, spark source mass spectroscopy was invoked to insure that there were no major impurities in the sample (total  $< 100$  ppm weight concentration). Once the crystal is clean, the surface is free of contaminants for 3–4 h at an operating pressure of  $2 \times 10^{-10}$  Torr.

The azimuthal motion of the sample mount allowed the crystal to be rotated such that the vector potential ( $\mathbf{A}$ ) of the light is parallel to either one of the two crystal mirror planes. Polarized light from the storage ring is used to identify the symmetry of the bulk and surface states as well as their intensities as a function of photon frequency. For example, we can separate the  $\Sigma_3$  and  $\Sigma_4$  surface states using  $s$ -polarized light with the polarization vector along the  $[001]$  and  $[1\bar{1}0]$  directions, respectively. Measurements at normal emission along the  $\Sigma$  symmetry line were made to probe the bulk band structure and to

separate the  $\Sigma_1$ ,  $\Sigma_3$ , and  $\Sigma_4$  initial state bands which are dipole allowed. Surface states are identified as stationary peaks separated from the bulk transition as the photon energy is varied.

Off-normal measurements are used to measure the dispersion of surface states. Selection rules allow the symmetry of the surface states away from  $\bar{\Gamma}$  to be determined. When the vector potential  $\mathbf{A}$  is contained in the  $(y, z)$  plane (see Fig. 1) and parallel to the  $[001]$  direction, the analyzer can be placed in the  $(y, z)$  plane to measure the even initial states or placed perpendicular to the  $(y, z)$  plane to measure odd initial states. The even states originate from  $\Sigma_3$  and  $\Sigma_1$ , while the odd states are from  $\Sigma_4$  and  $\Sigma_2$ . Similar measurements are done by rotating the crystal  $90^\circ$  such that  $\mathbf{A}$  is in the  $(x, z)$  plane and parallel to the  $[1\bar{1}0]$  direction. In this geometry, the even states probed originate from  $\Sigma_1$  and  $\Sigma_4$ , and the odd states come from  $\Sigma_3$  and  $\Sigma_2$ . Table I summarizes the initial states allowed by symmetry along  $\Gamma M$ . A detailed discussion on how to measure surface and bulk band dispersion can be found in review articles.<sup>17,18</sup>

Theoretical calculations were carried out using the local-density approximation<sup>19,20</sup> and the pseudopotential method.<sup>21</sup> In the present calculation the result of Ceperly and Alder<sup>22</sup> for the exchange-correlation functional in the parametrized forms given by Perdew and Zunger<sup>23</sup> was used. The ionic potentials in the solid are approximated by the nonlocal *ab initio* pseudopotentials derived by Bachelet *et al.*<sup>24</sup> The effective one-electron Schrödinger equation is solved by expanding the wave function in a physically complete basis set. The valence band of NiAl is characterized by a high density of  $sp$  electrons and nearly filled  $d$  bands, where the  $3d$  wave functions, highly localized on the Ni core region, need a prohibitively large number of reciprocal lattice vectors in a momentum-space expansion. Therefore, the conventional momentum-space formalism with a plane wave basis set or a mixed-basis set (Gaussian orbitals plus plane waves)<sup>25</sup> is not adequate for this system. We employ a real-space formulation of the mixed basis scheme<sup>26</sup> which is very effective in dealing with  $3d$  transition elements. In this scheme, a set of atomic  $d$  orbitals was derived which vanish outside a cutoff radius, allowing no intersite overlap between the localized basis functions. With this modification, the matrix elements in the band calculation and the valence charge density for the self-

TABLE I. Symmetry of the initial states.

$\mathbf{A} \parallel$	Normal emission	
	Dipole allowed	Dipole forbidden
$\bar{\Gamma} \bar{Y}$	$\Sigma_3, \Sigma_1$	$\Sigma_2$
$\bar{\Gamma} \bar{X}$	$\Sigma_4, \Sigma_1$	$\Sigma_2$
	Off-normal emission	
	Even states	Odd states
$\bar{\Gamma} \bar{Y}$	$\Sigma_3, \Sigma_1$	$\Sigma_4, \Sigma_2$
$\bar{\Gamma} \bar{X}$	$\Sigma_4, \Sigma_1$	$\Sigma_3, \Sigma_2$

consistent loop can be evaluated very accurately in real space.

In the present study, the NiAl(110) surface is simulated by a periodic array of thin films, each consisting of five atomic layers with vacuum separations of four-interlayer spacings in between slabs. The basis set for the supercell contains 25 optimized  $d$  orbitals and around 800 plane waves. We use 5  $k$  points in an irreducible sector of the Brillouin zone with a Gaussian weighting scheme<sup>27</sup> to accumulate the charge density. Iteration for self-consistency continues until the  $G$ -space components of the potential are stable to within 0.001 Ry. The changes of eigenvalues are within 0.005 eV and the total energy per unit cell is stable within to 0.05 mRy at the self-consistent range.

The electronic structures of both the unrelaxed and relaxed NiAl(110) surface were investigated. For the relaxed surface, the experimental geometry obtained from published LEED  $I$ - $V$  measurement<sup>1</sup> was used. This relaxation reduces the surface energy about 6.8 mRy per surface unit area and the surface work function changes from 4.55 eV (unrelaxed) to 4.39 eV (relaxed). Experimentally, the work function was determined to be 4.6 eV. Except for a small change in the binding energy for some surface states, the band structures of both systems look very similar on the whole. Hence, the relaxed surface is used in the description of the electronic structure of the surface states.

The surface-state and/or -resonance band structure in this calculation is divided into two subspaces according to the reflection symmetry about a surface mirror plane. Our convention is to denote a surface (resonance) state as one that contains more than 70% (50%) of its charge in the outermost surface layer and whose eigenvalue is either in a symmetry gap or very close to the edges of a gap. Following this convention several surface-state and/or -resonance bands were identified within 2 eV of the Fermi energy ( $E_F$ ). The character and dispersion of these bands are discussed in the following section.

### III. RESULT AND DISCUSSION

#### A. Bulk and surface band measurements: normal emission

Table I shows the allowed dipole transitions of the initial state bands along  $\Gamma M$ . Using both  $s$  and  $p$  polarization of the incident radiation and collecting photoelectrons emitted normal to the surface, three surface states are observed and the symmetries of these states are  $\Sigma_1$ ,  $\Sigma_3$ , and  $\Sigma_4$ . Figure 4 shows a set of typical photoemission spectra for several photon energies of these surface states. The energy distribution curves (EDC's) have been normalized so that the evolution of the peak intensities with photon energy can be followed. Their energies at  $\bar{\Gamma}$  are listed in Table II. Both the  $\Sigma_3$  and  $\Sigma_4$  surface states are well separated from the bulk bands and exhibit appreciable intensity over a wide range of photon energy as shown in Figs. 4(a) and 4(b). In these two figures, the surface states are indicated by the shaded peaks with  $\Sigma_4 = -1.08$  eV and  $\Sigma_3 = -1.12$  eV. Bulk transitions of the  $\Sigma_4$  and  $\Sigma_3$  states are indicated by arrows. Unlike the spectra displayed in Fig. 3(a), photoemission spectra in Fig. 4(b) show both the  $\Sigma_1$  and  $\Sigma_4$  bulk states since the  $\Sigma_1$  state has not been subtracted. Shown in Fig. 4(b) is a nondispersive peak at  $-0.65$  eV which appears in spectra taken below 40 eV photon energy. It is particularly intense at low photon energies. Although this peak shows no dispersion at normal emission, we do not assign this peak as a second  $\Sigma_4$  surface state for reasons that will be discussed in Sec. III C. The  $\Sigma_3$  surface state with a binding energy of 1.12 eV [Fig. 4(a)] is observed in spectra for photon energies of 12–56 eV. It is well separated from the bulk  $\Sigma_3$  band. In contrast, the  $\Sigma_1$  surface state was only observed at photon energies greater than 32 eV. This surface state is so close to the band edge at  $\bar{\Gamma}$  that it is partially overlapped by the bulk transition. Figure 4(c) shows that the  $\Sigma_1$  surface state (shaded peak) is a shoulder on the lower binding energy side of the bulk  $\Sigma_1$  peak

TABLE II. Characters and eigenvalues of surfaces states at  $\bar{\Gamma}$ . Their symmetries and functional dependences are present in the first column. The next two columns give the calculated eigenvalues in eV both for the unrelaxed surface and relaxed surface (with  $d_{Ni} = -6.0\%$  and  $d_{Al} = 4.0\%$ ) relative to the Fermi level. Experimental eigenvalues are given in the last column. Bottom: measured and calculated bulk band gap between  $M_2$  and  $M_5$ .

Surface states at $\bar{\Gamma}$	eV (unrelaxed)	eV (relaxed)	eV (expt)
$\Sigma_1(d_z)^a$	-1.23	-1.27	$-1.37 \pm 0.15$
$\Sigma_2(d_{xy})$	-1.22	-1.27	
$\Sigma_3(d_{yz})$	-1.04	-1.12	$-1.12 \pm 0.15$
$\Sigma_4(d_{xz})$	-0.98	-1.06	$-1.08 \pm 0.15$
	Calculation (eV)	Experiment (eV)	Difference (eV)
$M_2$	0.97	$0.85 \pm 0.20$	0.12
$M_5$	2.06	$1.76 \pm 0.10$	0.30
$M_5 - M_2$	1.09	0.91	0.18

<sup>a</sup>In the present definition, the  $z$  axis is along the surface normal direction, the  $x$  axis along the long Ni-Ni bridge in the  $[1\bar{1}0]$  direction, and the  $y$  axis along the short Ni-Ni bridge in the  $[001]$  direction.

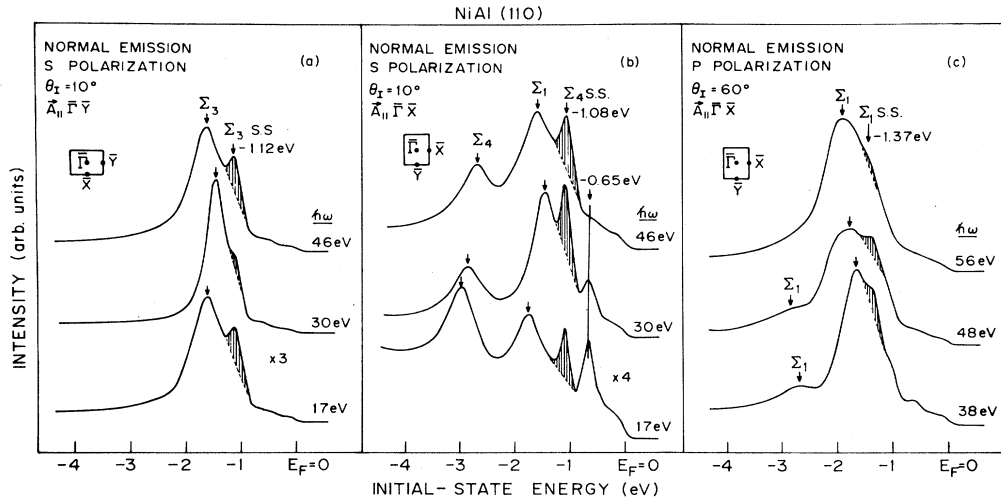


FIG. 4. Normal emission EDC's show (a)  $\Sigma_3$ , (b)  $\Sigma_4$ , and (c)  $\Sigma_1$  surface states exist over a wide range of photon energies. Surface states are shaded peaks and bulk transitions are indicated by arrows.

(indicated by the arrow).

The intensity variations with photon energy for the  $\Sigma_3$  and  $\Sigma_4$  surface states seen in the normal emission spectra are plotted in Figs. 5(a) and 5(b). These data are normalized by using the signal from a calibrated tungsten mesh. The intensity of the  $-1.08$ -eV  $\Sigma_4$  surface state shows a sharp peak at low photon energy (15 eV) and a broader maximum at 35 eV. The maximum at higher photon energy is typical of a surface state which has  $d$ -like character. In the same figure the intensity variation of the  $-0.65$ -eV state is plotted. The cross section for this peak is monotonically decreasing and thus, quite different from that observed for the  $\Sigma_4$  state. This behavior is more typical of a state with  $p$ -like wave function than that with  $d$ -like wave function. The intensity variation with photon energy for the  $\Sigma_3$  surface state at  $-1.12$  eV is shown in Fig. 5(b). This surface state displays similar behavior to that of the  $\Sigma_4$  surface state with two maxima, at 17 eV and at 40 eV.

The appearance of the sharp maximum in the cross section at low photon energy for both surface states could be a result of a surface-wave-induced interference effect.<sup>28</sup> There are several channels available for exciting an occupied initial state characterized by  $E(k_i)$  into a final state characterized by a plane wave traveling normal to the surface. The dominant channel is through normal emission while a second channel involves surface umklapp scattering. The transition matrix element for photoemission is given by

$$M_{fi} \propto \langle \psi_f | \mathbf{A} \cdot \mathbf{P} | \psi_i \rangle^2. \quad (1)$$

The final state of the electron  $\psi_f$  emitted normal to the surface can be written as follows:

$$\begin{aligned} \psi_f &= C_1 \psi_f^0(\mathbf{k}_{\parallel} = 0, E_f) + \sum_{\mathbf{g}_{\parallel}} C_{\mathbf{g}_{\parallel}} \psi_f^1(\mathbf{k}_{\parallel} = \mathbf{g}_{\parallel}, E_f) \\ &= \text{Normal emission} + \text{surface umklapp}, \end{aligned} \quad (2)$$

where  $\psi_f^0$  is the final-state wave function with  $\mathbf{k}_{\parallel} = 0$  and  $\psi_f^1$  is the final-state wave function with  $\mathbf{k}_{\parallel} = \mathbf{g}_{\parallel}$  ( $\mathbf{g}_{\parallel}$  being a surface reciprocal-lattice vector). Equation (2) shows that the final-state wave functions are composed of emission from normal ( $\mathbf{k}_{\parallel} = 0$ ) and from surface umklapp ( $\mathbf{k}_{\parallel} = \mathbf{g}_{\parallel}$ ) processes. Their transition strengths are weighted by the Fourier components  $C$ 's. Normally, the second term is small compared to the first term with the exception of the special case where the excited wave  $\psi_f^1$  is trapped in a surface Rydberg-like state (image potential state).<sup>29</sup> This condition occurs near the energy required for emergence of the photoemitted electron from  $\bar{\Gamma}$  of the second zone, resulting in a wave traveling parallel to the surface. In an ideal crystal, this surface state can escape only through umklapp scattering which involves  $\mathbf{k}_{\parallel} \rightarrow \mathbf{k}_{\parallel} \pm \mathbf{g}_{\parallel}$ , but  $\mathbf{k}_{\parallel} - \mathbf{g}_{\parallel} \approx 0$ . As a result of the umklapp processes, the emitted electron from the surface state will have  $\mathbf{k}_{\parallel} = 0$  and come out normal to the surface.

Since  $k_{\parallel}$  is conserved in crossing the surface, the energy for a surface wave traveling parallel to the surface is given by

$$E_{\parallel} = \frac{\hbar^2}{2m} (k_{\parallel})^2 \quad \text{with } k_{\parallel} \approx g_{\parallel}. \quad (3)$$

For the NiAl(110) SBZ, the surface reciprocal-lattice vectors ( $g_{\parallel}$ ) along the  $\bar{\Gamma}\bar{Y}$  and  $\bar{\Gamma}\bar{X}$  directions are  $2.18$  and  $1.54 \text{ \AA}^{-1}$ , respectively. Using these values of  $g_{\parallel}$ , we can make a rough estimate of the photon energy required to excite the occupied surface state at  $\bar{\Gamma}$  into an image potential surface state. This is given as follows:

$$\begin{aligned} \hbar\omega &= \frac{\hbar^2}{2m} (g_{\parallel})^2 + \phi \\ &= \begin{cases} 3.81(2.18)^2 + 4.6 = 23 \text{ eV} & \text{for } |g_{\parallel}| = 2.18 \text{ \AA}^{-1} \\ 3.81(1.54)^2 + 4.6 = 15 \text{ eV} & \text{for } |g_{\parallel}| = 1.54 \text{ \AA}^{-1} \end{cases}, \end{aligned} \quad (4)$$

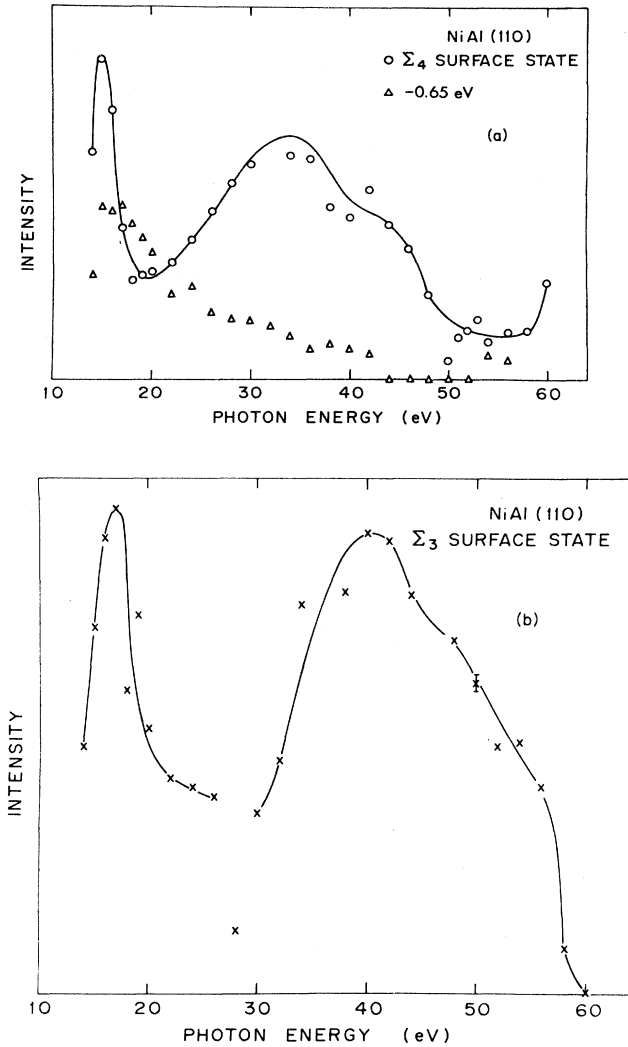


FIG. 5. Intensity variations of surface states with photon energy. (a)  $\Sigma_4$  surface state and the intensity variation of the  $-0.65$  eV peak. (b)  $\Sigma_3$  surface state.

where  $\phi$  is the work function. Since the intensities of the  $\Sigma_3$  and  $\Sigma_4$  surface states both peak near  $\hbar\omega = 15$  eV,  $g_{\parallel}$  involved in this process is along the  $[1\bar{1}0]$  direction. This could be due to the more efficient momentum coupling along the  $[1\bar{1}0]$  direction since the spatially varying charge distribution is larger in this direction than in the  $[001]$  direction. The fact that both the  $\Sigma_3$  and  $\Sigma_4$  surface states are coupled to the  $[1\bar{1}0]$  direction suggests a rather isotropic surface emission pattern.

#### B. Dispersions of surface-state bands: off-normal emission

At  $\bar{\Gamma}$ , the symmetries of the surface states are  $\Sigma_1$ ,  $\Sigma_3$ , and  $\Sigma_4$  as discussed in the previous section. As the analyzer is moved off-normal into a mirror plane, the symmetry of the surface state is reduced, and the wave function of each surface state can be discussed as either even or odd with respect to the reflection symmetry of

that mirror plane. If we define a set of orthogonal axes  $(x, y, z)$ , where  $z$  is the surface normal and  $x$  and  $y$  lie in the surface plane of the sample with  $x$  and  $y$  being along the  $[1\bar{1}0]$  and  $[001]$  directions, respectively [see Fig. 1(a)], the two mirror planes are the  $(y, z)$  and the  $(x, z)$  planes. The  $\Sigma_1$  surface state, characterized by a  $d_{z^2}$  wave function, is even with respect to reflection about the two mirror planes defined above. For the  $\Sigma_3$  and  $\Sigma_4$  surface states which have a  $d_{yz}$  and  $d_{xz}$  character, respectively, the wave functions can have either even or odd symmetry with respect to the reflection about the two mirror planes. The  $\Sigma_3$  surface state is even for emission to the  $(y, z)$  plane and is odd with respect to the  $(x, z)$  plane. Likewise, the  $\Sigma_4$  surface state is even with respect to the  $(x, z)$  plane and is odd with respect to the  $(y, z)$  plane. The  $\Sigma_2$  surface state, characterized by a  $d_{xy}$  wave function, is confined to the surface plane and its symmetry is odd with respect to both mirror planes. However, even though the  $\Sigma_2$  surface state cannot be observed at  $\bar{\Gamma}$ , there is still a possibility to observe it away from  $\bar{\Gamma}$ . The symmetry of the four surface states we have just discussed are summarized in the lower half of Table I. Away from  $\bar{\Gamma}$ , the parallel momentum ( $k_{\parallel}$ ) of the outgoing photoelectron can be related to the emission angle with respect to surface normal  $\theta_e$  by

$$k_{\parallel} = 0.512(\hbar\omega - E_b - \phi)^{1/2} \sin\theta_e \text{ \AA}^{-1}. \quad (5)$$

At a given photon energy, to observe even-symmetry states along the  $[001]$  direction ( $\bar{\Gamma} \bar{Y}$  in the SBZ), the sample is rotated such that  $\mathbf{A}$  is parallel to  $[001]$  and in the  $(y, z)$  plane. Even states along  $\bar{\Gamma} \bar{Y}$  are observed with the analyzer placed in the  $(y, z)$  plane, and odd states along  $\bar{\Gamma} \bar{X}$  are observed with the analyzer placed perpendicular to the  $(y, z)$  plane. The binding energy ( $E_b$ ) of the surface peak obtained in the EDC along with the emission angle give the  $k_{\parallel}$  of the surface state.

Figures 6(a)–6(d) show photoemission spectra taken at constant  $k_{\parallel}$ . The two EDC's shown in the left panel of Fig. 6 are taken at  $k_{\parallel} = 0.23 \pm 0.01 \text{ \AA}^{-1}$  ( $\frac{1}{3}$  of the SBZ) along  $\bar{\Gamma} \bar{X}$ . In this panel, the even state [Fig. 6(a)] has  $\Sigma_4$  symmetry and the odd state [Fig. 6(b)] has  $\Sigma_3$  symmetry. The right panel of Fig. 6 shows EDC's taken at the same  $k_{\parallel}$  ( $\frac{1}{4}$  of the SBZ) but along the  $\bar{\Gamma} \bar{Y}$  direction. In this panel, the even-symmetry state is  $\Sigma_3$  [Fig. 6(c)] and the odd-symmetry state is  $\Sigma_4$  [Fig. 6(d)]. This figure clearly shows that the observed surface states have the symmetry expected from  $d_{yz}(\Sigma_3)$  and  $d_{xz}(\Sigma_4)$  wave functions, i.e., the  $\Sigma_3$  surface state is even along  $\bar{\Gamma} \bar{Y}$  and odd along  $\bar{\Gamma} \bar{X}$ , while the  $\Sigma_4$  surface state is even along  $\bar{\Gamma} \bar{X}$  and odd along  $\bar{\Gamma} \bar{Y}$ .

Once the correct symmetry of the  $\Sigma_3$  and  $\Sigma_4$  surface states away from  $\bar{\Gamma}$  are known, the dispersions of these two surface bands can be determined. Figure 7(a) shows the dispersion of the  $\Sigma_3$  surface state, which has even symmetry along  $\bar{\Gamma} \bar{Y}$ . The spectra were taken at  $\hbar\omega = 42$  eV and the dispersion of this surface state is illustrated by the positions of the vertical bars. Starting at  $\bar{\Gamma}$ , this surface state has a binding energy of 1.12 eV and disperses towards the Fermi level. At  $k_{\parallel} = 0.5 \text{ \AA}^{-1}$  ( $\frac{1}{2}$  of the SBZ),

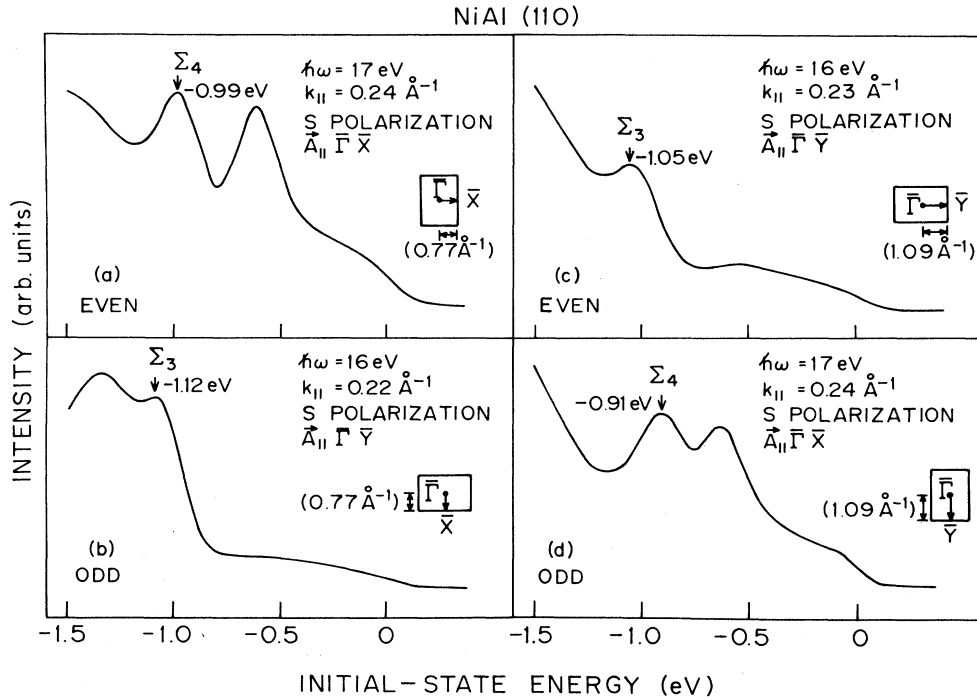


FIG. 6. Symmetry of surface states at  $k_{\parallel} = 0.23 \pm 0.01 \text{ \AA}^{-1}$ . Left panel shows EDC's along  $\bar{\Gamma}\bar{X}$ : (a)  $\Sigma_4$  surface state with even symmetry and (b)  $\Sigma_3$  surface state with odd symmetry. Right panel shows EDC's along  $\bar{\Gamma}\bar{Y}$ : (c)  $\Sigma_3$  surface state with even symmetry and (d)  $\Sigma_4$  surface state with odd symmetry.

the surface-state peak broadens which probably indicates that it has merged with the bulk bands and become a resonance.

The dispersion of the even-symmetry  $\Sigma_4$  surface state is shown in Fig. 7(b). All the EDC's shown in this figure are the "unsubtracted" *s*-polarized spectra showing both the  $\Sigma_1$  and  $\Sigma_4$  initial bulk states taken at  $\hbar\omega = 17 \text{ eV}$ . The  $\Sigma_4$  surface state has a binding energy of 1.08 eV at  $\bar{\Gamma}$ , and disperses towards the Fermi level at some finite  $k_{\parallel}$ . It remains sharp at all angles as it moves towards the Fermi level, indicating that this surface band remains in the bulk band gap. The peak at  $-0.65 \text{ eV}$  does not disperse but does change intensity. The dispersions of the odd-symmetry states are obtained in a similar manner along the  $\bar{X}-\bar{\Gamma}-\bar{Y}$  direction.

The  $\Sigma_1$  surface state is even along both  $\bar{\Gamma}\bar{Y}$  and  $\bar{\Gamma}\bar{X}$ . The dispersion of this surface state along the  $\bar{\Gamma}\bar{X}$  direction was measured at 38 eV photon energy. However, the energy of this surface state is too close to the bulk state to allow a very precise determination of the dispersion. Away from the zone center, this surface state becomes a resonance state and disperses away from the Fermi level. Near  $k_{\parallel} = 0.3 \text{ \AA}^{-1}$ , the  $\Sigma_1$  surface peak is no longer observable in the photoemission spectrum, indicating that it probably merges with the bulk  $\Sigma_1$  state.

The calculated  $\Sigma_2$  surface state is odd along both  $\bar{\Gamma}\bar{Y}$  and  $\bar{\Gamma}\bar{X}$ . The wave function of this surface state has  $d_{xy}$  character and cannot be observed in the first surface Brillouin zone by normal emission. In principle, this surface

state could be observed away from  $\bar{\Gamma}$ . However, the coupling between the in-plane  $d_{xy}$  wave function of the  $\Sigma_2$  surface state to the plane wave free-electron final state is generally very small, and this may explain the failure to observe the  $\Sigma_2$  surface state in the off-normal photoemission spectra.

### C. Comparison between experiment and theory

The symmetries and binding energies of the measured and calculated surface states of NiAl(110) at  $\bar{\Gamma}$  are summarized in Table II. This table shows that the experimental and theoretical binding energies of the surface states are in good agreement. The calculated binding energies of the  $\Sigma_3$  and  $\Sigma_4$  states are smaller than those of  $\Sigma_1$  and  $\Sigma_2$ . The main contribution to this difference comes from the charge redistribution in the surface region. The (110) truncation of bulk NiAl leaves two hollows at the short and long bridge Ni—Ni regions in the surface plane. A high density of nearly free electrons from the surface Al sites flow into these low-density regions to reduce the surface charge corrugation. Since the localized charge densities of  $\Sigma_3$  and  $\Sigma_4$  states extend to the short and long Ni—Ni bridge, respectively, they feel a stronger repulsive force from the enhanced *sp* electrons than do the  $\Sigma_1$  and  $\Sigma_2$  surface states, which are localized over the Ni atoms and in the Ni—Al bridge region, respectively. This repulsion results in weaker binding energies of the  $\Sigma_3$  and  $\Sigma_4$  surface states. Charge density plots

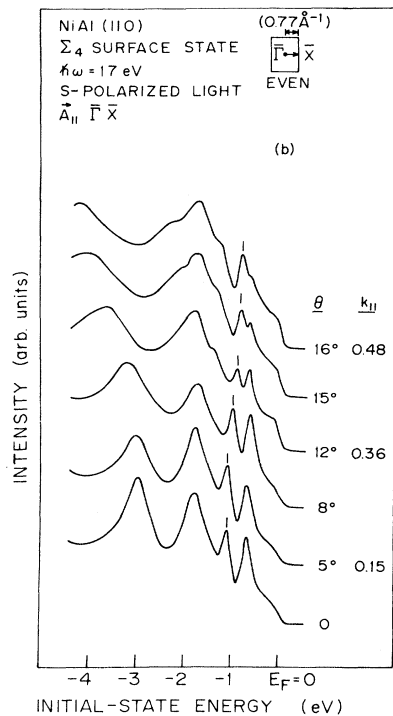
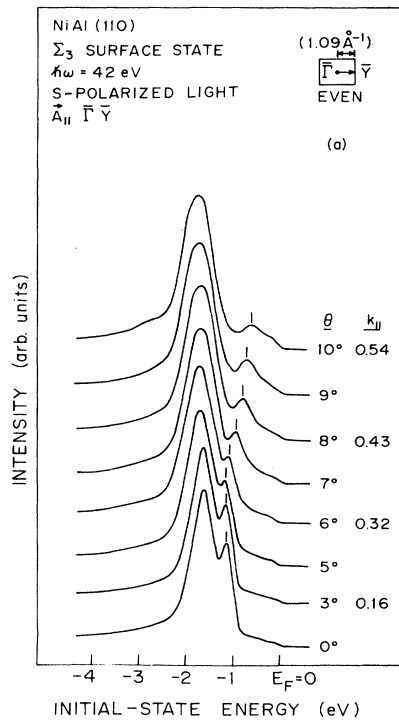


FIG. 7. Dispersions of surface states. (a)  $\Sigma_3$  surface state with even symmetry along  $\bar{\Gamma}-\bar{Y}$ ; (b)  $\Sigma_4$  surface state with even symmetry along  $\bar{\Gamma}-\bar{X}$ .

of these two surface states are displayed in Fig. 8. For both the  $\Sigma_3$  and  $\Sigma_4$  surface states, the  $d$ -like charge lobes extending towards the Ni—Ni bridge are distorted due to the creation of a surface, and consequently the symmetry of the wave function is reduced.

Figures 9(a)–9(d) show even and odd projection along the  $\bar{X}-\bar{\Gamma}-\bar{Y}$  directions. Since all of the calculated surface states exist in the band gap located 1 eV below the Fermi level, we only show this portion of the bulk projection. Due to differences between the measured and calculated bulk bands, the bulk projections are plotted in different figures. Figures 9(b) and 9(d) show the projections of bulk bands and surface states from theory and Figs. 9(a) and 9(c) show those from experiment. The dashed lines in Figs. 9(a) and 9(c) show the expected position of the bulk band edge since detailed measurements in these regions had not been performed. In Figs. 9(b) and 9(d), surface (resonance) bands are indicated by solid (dashed) lines and are labeled as  $A_n(a_n)$ ,  $B_n(b_n)$ , etc. for even (odd) states with  $n$  being the band index. Their wave-function symmetry and energy at  $\bar{\Gamma}$  are given in Table II. To label the symmetry points and lines in the SBZ, we use the subscripts 1 and 2 to denote even and odd subspaces, respectively. Figures 9(b) and 9(d) show that the dispersion of these surface states is different along the two major symmetry directions. Nearly dispersionless surface-state bands are observed along the  $[1\bar{1}0]$  or  $\bar{\Gamma}-\bar{X}$  direction, where interaction between neighboring Ni atoms is small. On the other hand, strong interactions between Ni atoms occurs along the  $[001]$  or  $\bar{\Gamma}-\bar{Y}$  direction due to the shorter atomic distance resulting in more dispersive bands.

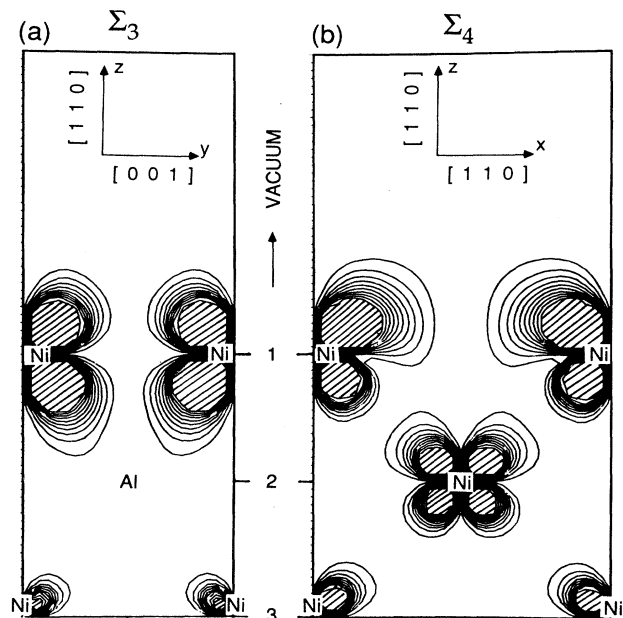


FIG. 8. Charge density plots of (a)  $\Sigma_3$  and (b)  $\Sigma_4$  surface states.

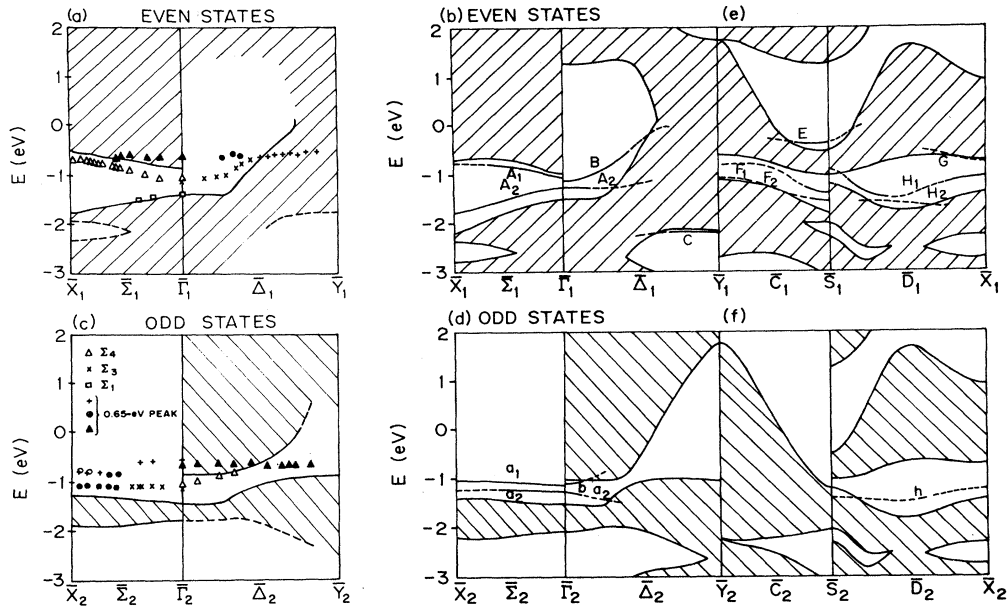


FIG. 9. Bulk even and odd projections along  $\bar{X}-\bar{\Gamma}-\bar{Y}$  and  $\bar{Y}-\bar{S}-\bar{X}$  showing surface-state dispersions. Experimental data points are given by symbols. Results of calculations are indicated by solid and dashed lines (see text for band labeling). (a) and (c) Measured even and odd surface bands along  $\bar{X}-\bar{\Gamma}-\bar{Y}$ , (b) and (d) calculated even and odd surface bands. Symbols enclosed by circles in (a) and (c) are results of measurements taken in the second SBZ. (e) and (f) Calculated even and odd surface band dispersions along  $\bar{Y}-\bar{S}-\bar{X}$ .

Along the  $\bar{\Sigma}_1$  symmetry line [Fig. 9(b)], the calculated bulk band gap is widened from 0.5 eV at  $\bar{\Gamma}$  to 1.5 eV at  $\bar{X}$ . The charge distribution for bands  $A_1$  and  $A_2$  in the even-symmetry subspace has a main orbital character of  $d_{xz}$  ( $\Sigma_4$ ) and  $d_{z^2}$  ( $\Sigma_1$ ), respectively, at  $\bar{\Gamma}$ . Going from  $\bar{\Gamma}_1$  to  $\bar{X}_1$ , these orbitals hybridize and the orbital characters reverse to  $d_{z^2}$  and  $d_{xz, x^2-y^2}$ , respectively, at  $\bar{X}$ . The measured band dispersions along  $\bar{\Gamma}_1$  to  $\bar{X}_1$  (indicated by  $\Delta$  and  $\square$ ) agree very well with the calculated  $A_1$  and  $A_2$  bands. The dispersion of the  $A_1$  band ( $\Sigma_4$ ) is shown in Fig. 7(b) whereas its symmetry is shown in Fig. 4(b) at  $\bar{\Gamma}$  and in Fig. 6(a) away from  $\bar{\Gamma}$ . The dispersion of the  $\Sigma_1$  surface state (i.e., the  $A_2$  band) is observed only near  $\bar{\Gamma}$  and it apparently merges with the bulk  $\Sigma_1$  band away from  $\bar{\Gamma}$ .

Along  $\bar{\Gamma}_1\bar{Y}_1$ , a bulk gap exists only in a narrow region near  $\bar{\Gamma}$  [Fig. 9(b)]. The surface band is more dispersive due to the shorter atomic distance in this wave vector direction. Surface band **B** loses its surface character in the middle of the SBZ where it merges into a bulk band. The charge density distribution along this band shows a main character of  $d_{yz}$  ( $\Sigma_3$ ) at  $\bar{\Gamma}$  with an increasing admixture of the  $sp$  character away from  $\bar{\Gamma}$ , and finally a  $d_{x^2-y^2}$  character when it merges into a bulk band. The calculated dispersion of this band **B** reproduces the experimentally measured band dispersion (indicated by  $\times$ ) very well as shown in Fig. 9(a). The measured dispersion of this band is shown in Fig. 7(a) and its symmetry at  $\bar{\Gamma}$  and away from  $\bar{\Gamma}$  are shown in Figs. 4(a) and 6(c), respectively. In our calculation, we also found a strong surface state (band **C**) at  $-2.2$  eV which extends from  $\bar{Y}_1$  to the

middle of  $\bar{\Delta}_1$  with a main character of  $d_{yz}$ . Experimentally, the search for this surface state is different since it does not originate at  $\bar{\Gamma}$ . In the photoemission spectra collected along  $\bar{\Gamma}\bar{Y}$ , we did not observe a surface state which can be assigned to band **C** as calculated.

In the odd-symmetry subspace shown in Fig. 9(d), bands  $a_1$  and  $a_2$  are flat along the  $\bar{\Sigma}_2$  symmetry line of the SBZ. The charge density retains the same  $d_{xz}$  and  $d_{xy}$  character, respectively, over the whole bands. The  $a_2$  band ( $\Sigma_2$ ) is not observed experimentally. Band  $a_1$ , however, shows very good agreement with the measured band dispersion ( $\Sigma_3$ ) as indicated by data points shown as  $\times$  in Fig. 9(c). Data points denoted by  $\otimes$  are from measurements made in the second SBZ folded back to the first zone. Along the  $\bar{\Delta}_2$  symmetry direction, the two odd bands are **b** and  $a_2$ . The measured dispersion of band **b** [Fig. 9(c)] with  $\Sigma_4$  symmetry at  $\bar{\Gamma}$  is reproduced quite well by the calculation. The data points for band **b** are denoted by open triangles. Band  $a_2$  again is not observed experimentally along the  $\bar{\Delta}_2$  symmetry line.

Figures 9(e) and 9(f) show the calculated surface bands along  $\bar{Y}-\bar{S}-\bar{X}$  in the SBZ. No attempts were made to measure dispersions of the surface bands along these symmetry directions. The main features of the surface bands along the  $\bar{Y}-\bar{S}-\bar{X}$  line in Figs. 9(e) and 9(f) are very similar to those along  $\bar{X}-\bar{\Gamma}-\bar{Y}$ . With the exception of one resonance band of odd symmetry which extends from  $\bar{S}_2$  to the middle of  $\bar{Y}_2$  with the binding energy of 4.5 eV and a  $d_{x^2-y^2}$  character [not shown in Fig. 9(f)], all surface-resonance bands are distributed within 2 eV below the Fermi level. The surface states along  $\bar{Y}-\bar{S}-\bar{X}$  also have

strong  $d$  character. A weakly bound surface band  $E$  (main character,  $d_{z^2, x^2-y^2}$ ) exists just below the Fermi energy at the bottom of an absolute gap around  $\bar{S}$ . The surface band  $H_1(d_{yz})$  and the resonance bands  $G(d_{z^2})$ ,  $H_2(d_{z^2, x^2-y^2})$ , and  $h(d_{xy})$  are also found in another absolute gap on the  $\bar{S}-\bar{X}$  line. An even-symmetry gap around  $-1$  eV on the  $\bar{Y}-\bar{S}$  line contains two resonance bands  $F_1(d_{xz})$  and  $F_2(d_{z^2, x^2-y^2})$ .

From the above discussion, the energy positions and dispersions of the surface bands show good qualitative agreement between theory and experiment. The good agreement in Table II is surprising in view of the self-energy shifts of  $\leq 0.5$  eV found for bulk emission from the  $d$  bands.<sup>14</sup> The differences in the experimental bulk band energies when compared to theory (see bottom of Table II) are presumably due to the effect of the excitation process.<sup>14</sup> Excited states are measured by photoemission while the ground state is calculated. The differences in energy positions between the measured and calculated band gap (between  $M_2$  and  $M_5$ ), which contain the surface states at  $\bar{\Gamma}$ , is given in the bottom of Table II.

The fact that the agreement between theory and experiment is very good for the surface states coupled with the systematic differences between theory and experiment for the bulk bands<sup>14</sup> creates a problem in discussing the positioning of the surface states within the bulk gaps. For example, in the even bulk projections [Figs. 9(a) and 9(b)], the  $\Sigma_3$  and  $\Sigma_4$  surface states at  $\bar{\Gamma}$  are found in the middle of the experimental bulk band gap while the theory shows that these two surface states are very close to the bulk band edge. Another difference between theory and experiment is found in the  $\Sigma_1$  surface state. The measured  $\Sigma_1$  surface state at  $\bar{\Gamma}$  is very close to the bulk band edge as shown in Fig. 9(a), whereas the calculated  $\Sigma_1$  surface state lies in the middle of the band gap. Similar discrepancies are found in the odd projections [Figs. 9(c) and 9(d)] for the  $\Sigma_3$  and  $\Sigma_4$  surface states. There are at least two possible explanations for the disagreement between theory and experiment concerning the position of the surface states within the bulk gaps. The first is an energy potential problem with the numerical procedure, and the second is a physical phenomena ignored in the theory. The numerical problem arises because we are comparing a five-layer-slab calculation for the position of the surface states with a bulk calculation for the bulk band gaps. Procedures for integrating the bulk density of states in the bulk calculation and the density of states in the slab calculation to obtain the Fermi energy can result in a shift (or uncertainty) in the energy position of the surface states. If this is the explanation, the remarkable agreement seen in Table II is fortuitous. The second explanation is that the self-energy correction to the single particle energy is different in the surface than in the bulk.

The nature of the photoemission peak with binding energy of 0.65 eV has not been discussed so far. Its energy position in the bulk band projections [Figs. 9(a) and 9(c)] is shown by closed triangles along symmetry lines  $\bar{\Sigma}_1$  and  $\bar{\Delta}_2$ , and by + along  $\bar{\Delta}_1$  and  $\bar{\Sigma}_2$ . (The  $\oplus$  along  $\bar{\Sigma}_2$  are data points folded back from second zone.) Figures 9(a) and 9(b) show that this state exists both in the bulk continu-

um as well as inside the band gap. Except for intensity variation in the photoemission spectra taken along different symmetry directions, there is no well-defined symmetry of this state at  $\bar{\Gamma}$  and along  $\bar{X}-\bar{\Gamma}-\bar{Y}$ . The near-dispersionless nature of this state suggests that it is atomlike, with a very localized wave function. However, the cross section of this state shown in Fig. 5(a) is characteristic of a  $p$ -like wave function. It could be an extrinsic surface state or a localized defect state except for the fact that it is insensitive to surface contamination by carbon monoxide and oxygen. In the following, we offer a possible explanation for the existence of this peak in the photoemission spectra. For the bulk Ni-Al alloy system, the  $\beta'$  phase which has the CsCl structure exists between 45 and 60 at. % Ni. For a 1:1 stoichiometry, there is one Ni and one Al atom per unit cell. However, deviations from this stoichiometry with a Ni concentration greater than 50 at. % result in having Ni atoms occupy Al sites substitutionally.<sup>30</sup> In preparing the clean surface, the sputtering process results in a loss of Al atoms in the selvedge region. Although subsequent annealing results in the diffusion of Al from the bulk to this region, it is impossible to conclude that the outermost layers have the exact 1:1 stoichiometry. Thus a small concentration of excess Ni atoms occurring at the surface could shift the Ni  $d$  density of states towards the Fermi level leading to an observable feature in the photoemission spectra. We suggest that the  $-0.65$ -eV peak in the  $\Sigma_4$  spectra, Fig. 4(b), is due to excess Ni at the surface. Since the photoemitted intensity in the  $\Sigma_3$  spectra is approximately 11 times that of the  $\Sigma_4$  spectra, it is not unreasonable that the  $-0.65$ -eV feature is not observed in Fig. 4(a).

To summarize the above discussion of the relaxed surface-resonance band structure of the NiAl(110) surface, we compare in Fig. 10 the calculated density of states (DOS) of the five-layer slab (dashed curve) with the corresponding DOS of bulk NiAl. Although the overall characteristics of the two curves are very similar, the slab DOS shows two new features as indicated by  $a$  and  $b$  in Fig. 10. Peak  $a$  is attributed to a surface state at  $-1.0$

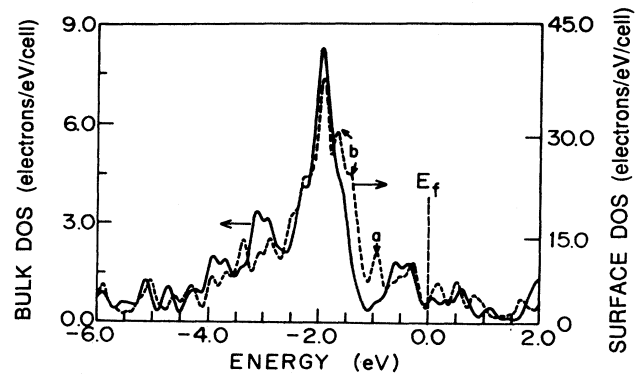


FIG. 10. Total density of states (DOS) of NiAl(110) calculated from a five-layer slab (dashed curve). The DOS from bulk NiAl is also shown for reference (solid curve).

eV and peak *b* to a *d*-resonance state near the lower gap edge. The surface-state peak in the DOS curve is predominantly *d*-like, and it contains the  $\Sigma_2$ ,  $\Sigma_3$ , and  $\Sigma_4$  surface states. The resonance peak is mainly from the surface-state band including the  $\Sigma_1$  state. It is easy to see from Fig. 10 that if an appropriate amount of the bulk DOS (solid curve) is subtracted from the five-layer DOS, the remaining true surface DOS curve will be shifted towards the Fermi level. Experimentally, it is possible to create simulated surface and bulk DOS curves by summing many angle and photon energy spectra with either the bulk or surface-state peaks removed. When this is done the first moment of the constructed surface DOS is shifted towards the Fermi level by  $\approx 0.5$  eV compared to the bulk DOS. This shift in the surface DOS suggests that the surface Ni and Al atoms in the alloy have recovered some of their atomic character. However, the magnitude of the shift in the surface DOS is not large enough to affect the DOS at the Fermi level. Therefore, the magnetic property of NiAl(110) is expected to be the same as the bulk, i.e., nonmagnetic.

#### IV. CONCLUSION

The electronic properties of the NiAl(110) surface are characterized by surface states existing throughout most

of the SBZ. The experimental results were compared with theoretical calculations, which qualitatively reproduce the energy positions of the surface-resonance states. We found that the filled *d* band, a characteristic of the bulk NiAl, was also present for the surface, indicating that the (110) surface has the same magnetic properties as the bulk. The agreement between theory and experiment is encouraging, especially considering the complexities associated with an alloy surface. Yet, there is one remaining discrepancy: the position of the surface states with respect to the bulk band edges. This problem may be associated with a difference in the self-energy near the surface where there is a rapid variation in the charge density profile.

#### ACKNOWLEDGMENTS

This work is supported at the Laboratory for Research on the Structure of Matter at the University of Pennsylvania by the National Science Foundation (NSF), Materials Research Laboratory Program Grant No. DMR-85-19059 and at Oak Ridge National Laboratory (ORNL) by the Division of Materials Sciences, Office of Basic Energy Sciences, Department of Energy, under Contract No. DE-AC05-84OR21400 with Martin Marietta Energy Systems, Inc.

- 
- <sup>1</sup>H. L. Davis and J. R. Noonan, *Phys. Rev. Lett.* **54**, 566 (1985).  
<sup>2</sup>S. M. Yalisove and W. R. Graham, *Surf. Sci.* **183**, 556 (1987).  
<sup>3</sup>S. P. Chen, A. F. Voter, and D. J. Srolovits, *Phys. Rev. Lett.* **57**, 1308 (1986).  
<sup>4</sup>M. H. Kang and E. J. Mele, *Phys. Rev. B* **36**, 7371 (1987).  
<sup>5</sup>J. I. Lee, C. L. Fu, and A. J. Freeman, *Phys. Rev. B* **36**, 9318 (1987).  
<sup>6</sup>S.-C. Lui, J. M. Mundenar, E. W. Plummer, M. Mostoller, R. M. Nicklow, D. M. Zehner, W. K. Ford, and J. Erskine, in *Physical and Chemical Properties of Thin Metal Overlayers and Alloy Surfaces*, edited by D. M. Zehner and G. W. Goodman [Mater. Res. Soc. Symp. Proc. **83**, 47 (1987)].  
<sup>7</sup>M. Mostoller, R. M. Nicklow, D. M. Zehner, S.-C. Lui, J. M. Mundenar, and E. W. Plummer, *Phys. Rev. B* (to be published).  
<sup>8</sup>J. M. Mundenar, R. H. Gaylord, S.-C. Lui, E. W. Plummer, L. Sneddon, D. M. Zehner, and W. K. Ford, in Ref. 6, p. 59.  
<sup>9</sup>D. M. Zehner and G. R. Gruzalski, in Ref. 6, p. 199.  
<sup>10</sup>M. W. Finnis and V. Heine, *J. Phys. F* **4**, L37 (1974).  
<sup>11</sup>H. L. Davis and J. R. Noonan, *Surf. Sci.* **126**, 245 (1983).  
<sup>12</sup>J. A. Seitchik and R. H. Walmsley, *Phys. Rev.* **131**, 1473 (1963); J. J. Spokas, *Phys. Rev. B* **1**, 2523 (1970).  
<sup>13</sup>For the density of states of Al, Ni, and Cu, see V. L. Moruzzi, J. F. Janak, and A. R. Williams, *Calculated Electronic Properties of Metals* (Pergamon, New York, 1978).  
<sup>14</sup>S.-C. Lui, J. W. Davenport, E. W. Plummer, D. M. Zehner, and G. W. Fernando (unpublished).  
<sup>15</sup>B. P. Tonner, *Nucl. Instrum. Methods* **172**, 133 (1980).  
<sup>16</sup>C. L. Allyn, T. Gustafsson, and E. W. Plummer, *Rev. Sci. Instrum.* **49**, 1197 (1978).  
<sup>17</sup>E. W. Plummer and W. Eberhardt, *Adv. Chem. Phys.* **49**, 533 (1982).  
<sup>18</sup>F. Himpsel, *Adv. Phys.* **32**, 1 (1983).  
<sup>19</sup>H. Hohenberg and W. Kohn, *Phys. Rev.* **136**, B864 (1964).  
<sup>20</sup>W. Kohn and L. J. Sham, *Phys. Rev.* **140**, A1133 (1965).  
<sup>21</sup>For a review, see M. L. Cohen, *Phys. Scr. T* **1**, 5 (1982).  
<sup>22</sup>D. M. Ceperley and B. J. Alder, *Phys. Rev. Lett.* **45**, 566 (1980).  
<sup>23</sup>J. P. Perdew and A. Zunger, *Phys. Rev. B* **23**, 5048 (1981).  
<sup>24</sup>G. B. Bachelet, D. R. Hamann, and M. Schluter, *Phys. Rev. B* **26**, 4199 (1982); **29**, 2309(E) (1984).  
<sup>25</sup>S. G. Louie, K. M. Ho, and M. L. Cohen, *Phys. Rev. B* **19**, 1774 (1979).  
<sup>26</sup>M. H. Kang, R. C. Tatar, E. J. Mele, and P. Soven, *Phys. Rev. B* **35**, 5457 (1987).  
<sup>27</sup>C. L. Fu and K. M. Ho, *Phys. Rev. B* **28**, 5480 (1983).  
<sup>28</sup>P. A. Dowben, D. Heskett, E. W. Plummer, Y. Sakisaka, T. N. Rhodin, and C. Umrigar, *Phys. Rev. Lett.* **53**, 1493 (1984).  
<sup>29</sup>E. G. McRae, D. Aberdam, R. Baudoing, and Y. Gauthier, *Surf. Sci.* **78**, 518 (1978).  
<sup>30</sup>A. J. Bradley and A. Taylor, *Proc. R. Soc. (London)* **159**, 56 (1937).